PHILOSOPHICAL TRANSACTIONS OF THE ROYAL SOCIETY A MATHEMATICAL, PHYSICAL & ENGINEERING SCIENCES

Magnetic localization and magnetoresistance in mixed–valence manganites and related ferromagnetic oxides

J. M. D. Coey

Phil. Trans. R. Soc. Lond. A 1998 **356**, 1519-1541
doi: 10.1098/rsta.1998.0233

The Royal Society

Magnetic localization and magnetoresistance in mixed-valence manganites and related ferromagnetic oxides

By J. M. D. Coey

Department of Physics, Trinity College, Dublin 2, Ireland and Center for Magnetic Recording Research, University of California, San Diego, CA 92093, USA

The electronic structure and properties of ferromagnetic mixed-valence manganites with the perovskite structure are briefly reviewed. The importance of disorder-induced localization is emphasized, and it is proposed that magnetic disorder is effective in this sense on three different length scales. First, spin disorder on the interatomic scale (*ca.* 1 nm) contributes to localization in the paramagnetic state above the Curie point. Second, fluctuations in the ferromagnetic order and electron density (*ca.* 10 nm) contribute to localization in the 'bad metal' state found in most manganites below the Curie point. Third, in granular systems (*ca.* 100 nm), electrons are inhibited from tunnelling between grains by misalignment of their ferromagnetic axes. The latter effects are studied in pressed powder compacts of $(La_{0.7}Ca_{0.3})MnO_3$ and the other half-metallic systems Fe_3O_4 and CrO_2. Here the resistance is entirely due to the interparticle contacts. The new phenomenon of powder magnetoresistance is presented, where magnetoresistance ratios of 50% are observed in pressed powder.

Keywords: powder magnetoresistance; chromium dioxide; magnetite; magnetic localization; Coulomb gap; spin-polarized tunnelling

1. Introduction

Mixed-valence manganites with the perovskite structure have been studied for almost 50 years. Early research was motivated by a need to develop insulating ferromagnets with a large magnetization for high-frequency applications. Recent work has been driven by a desire to understand and exploit the large negative magnetoresistance effect which appears near the Curie temperature. The manganites have potential as solid electrolytes, catalysts, sensors and novel electronic materials. The system offers a degree of chemical flexibility, which permits the relations between structure, electronic and magnetic properties to be examined in a systematic way. Rich electronic phase diagrams reflect the fine balance of interactions which together determine the electronic ground state.

The extensive literature on the physical properties of mixed-valence manganites has recently been reviewed by Coey *et al.* (1998*c*), and there are short reviews on colossal magnetoresistance and theoretical aspects by Ramirez (1997) and Nagaev (1996), respectively. The reader is referred to the first of these for detailed literature references. Broadly speaking, manganite research has developed in three stages; the first stage, beginning with the work of Jonker & van Santen (1950) was based on measurements of polycrystalline ceramics; the second stage, beginning with the work of

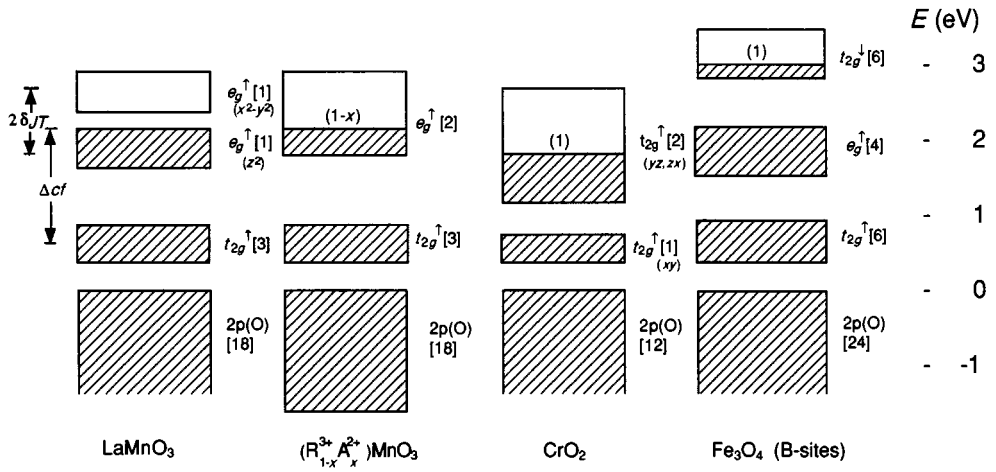

Figure 1. Schematic band structure of $LaMnO_3$, $(R_{0.7}A_{0.3})MnO_3$, Fe_3O_4 and CrO_2.

Searle & Wang (1970) was based on measurements of single crystals; the third stage, beginning with the work of von Helmholt *et al*. (1993) and Chahara *et al*. (1993) five years ago, was based on thin films. The research has given rise to important physical concepts, including double exchange and the Jahn–Teller polaron, as well as the discovery of new phenomena, including optically and electrically induced magnetic phase transitions, colossal intrinsic magnetoresistance and grain-boundary magnetoresistance. Here we focus on the last two of these topics, and introduce the new idea of powder magnetoresistance (PMR).

First, we place the manganites in context, from the points of view of crystal structure, electronic structure and magnetic order. We will discuss the ferromagnetic manganites in relation to two other conducting oxides, magnetite and chromium dioxide. The class of ferromagnetic metallic oxides is a small one.

Mixed-valence manganites are solid solutions based on an $RMnO_3$ end-member, where R is a rare earth ion. In the ABO_3 perovskite structure, Mn is on the B-site in octahedral oxygen coordination, with crystal-field splitting Δ_{cf} between the t_{2g} and e_g one-electron orbitals. $LaMnO_3$ is a planar A-type antiferromagnet with a Néel temperature of 130 K. The simple cubic perovskite structure undergoes a double distortion in the end member, reducing the symmetry to orthorhombic (O′ structure). There is a buckling of the MnO_6 octahedral array to accomodate the size discrepancy between R^{3+} and O^{2-}, and a chequerboard distortion to the octahedra in the basal plane that is due to the Jahn–Teller effect for Mn^{3+}, which splits the $e_g^{\uparrow}$ orbitals (d_{z^2} and $d_{x^2-y^2}$). The Jahn–Teller splitting δ_{JT} is slightly greater than the e_g bandwidth W (Pickett & Singh 1996). $LaMnO_3$ is an insulator, with a small activation energy *ca.* 0.1 eV. Although there is an indirect gap in the e_g density of states, this does not really explain the activated conduction. The oxide is unlikely to be perfectly stoichiometric; there will often be a cation deficiency arising from the preparation conditions, and the fact that the material is semiconducting suggests that small numbers of holes in the $e_g^{\uparrow}$ band are localized by disorder, with a mobility edge *ca.* 0.1 eV below the Fermi level. With sufficient non-stoichiometry in the form of cation vacancies,

$$(\mathrm{RMn})_{1-\delta}\mathrm{O}_3, \tag{1.1}$$

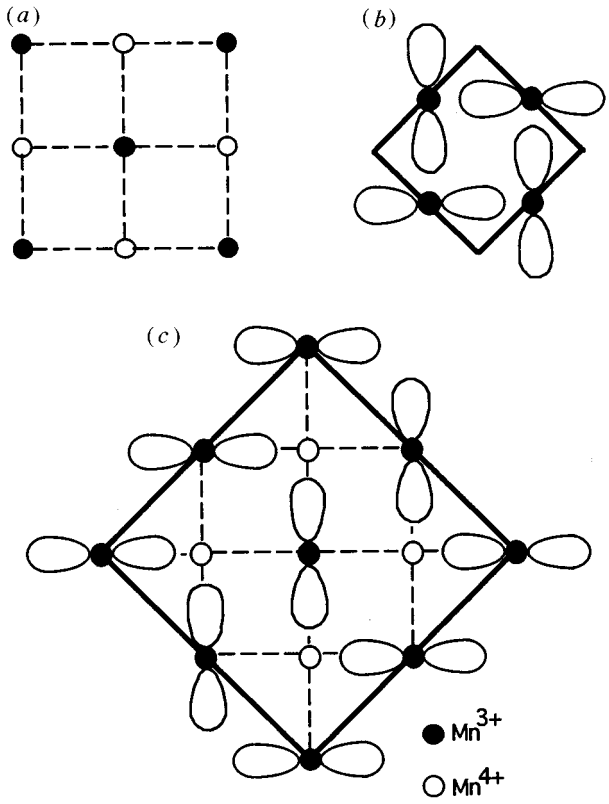

Figure 2. Schematic illustrations (*a*) charge order, (*b*) orbital order and (*c*) combined charge and orbital order in the basal plane of a manganite.

Table 1. *Estimates of characteristic energies in* $LaMnO_3$ (*in* eV)

U_{dd}	4.0	J_H	1.0
U_{pd}	4.5	Δ_{cf}	1.8
		δ_{JT}	0.6
$W = 12t$	1.0	$\|J_{ij}\|$	0.001

with $\delta > 0.05$, the material with R = La becomes a ferromagnetic metal. The value $\delta = 0.04$ corresponds to hole doping (Mn^{4+} content) of 0.25.

Similarly, on substituting a divalent or monovalent cation for La, some of the manganese also formally becomes Mn^{4+}; $3d^3$, and as long as the band remains Jahn–Teller split, the process may be thought of as hole doping of a semiconductor. At a critical doping the carriers become delocalized and the Jahn–Teller distortion becomes dynamic, and then disappears. The oxide usually becomes metallic, but it exhibits a metal–insulator transition near the Curie point. Unlike a normal metal–insulator transition, where the low-temperature phase is insulating, and the high-temperature phase is metallic, here it is the other way round. Since this transition occurs near the Curie point, there is every reason to believe the transition is of magnetic origin.

The formula of the mixed-valence manganites with divalent cation doping may be

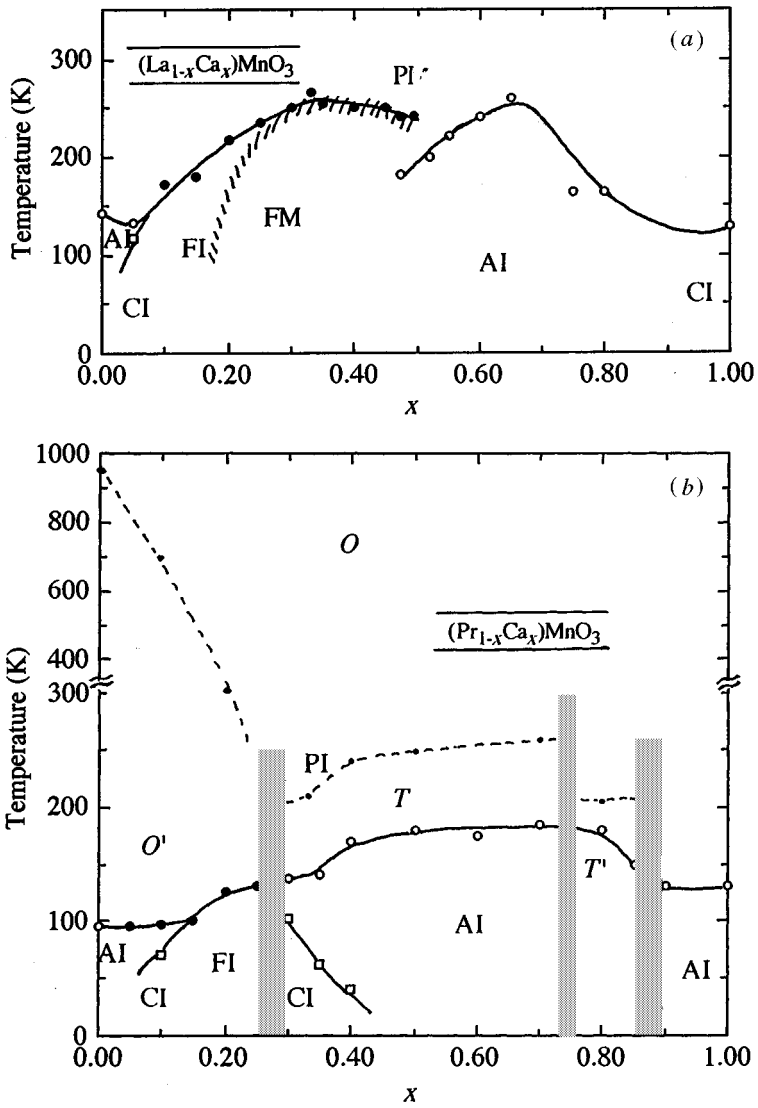

Figure 3. Phase diagrams for mixed-valence manganite systems La–Ca (top) and Pr–Ca (bottom). The phases are PI (paramagnetic insulator), AI (antiferromagnetic insulator), CI (canted antiferromagnetic insulator), FI (ferromagnetic insulator), FM (ferromagnetic metal). The hatched line represents the metal–insulator transition. Dashed lines are structural phase transitions, and italic letters denote the structure: O, orthorhombic; O', orthorhombic with Jahn–Teller distortion; R, rhombohedral; T, T', tetragonal. Grey indicates a two-phase region.

written

$$(\mathrm{R}^{3+}_{1-x}\mathrm{A}^{2+}_{x})(\mathrm{Mn}^{3+}_{1-x}\mathrm{Mn}^{4+}_{x})\mathrm{O}_3. \tag{1.2}$$

The band structures of the end-member and that of a ferromagnetic $x = 0.3$ compound are shown schematically in figure 1, where they are compared with those of CrO_2 and Fe_3O_4. What these oxides have in common is a d-band structure where there is a spin-polarized core of localized 3d electrons, and a delocalized spin-

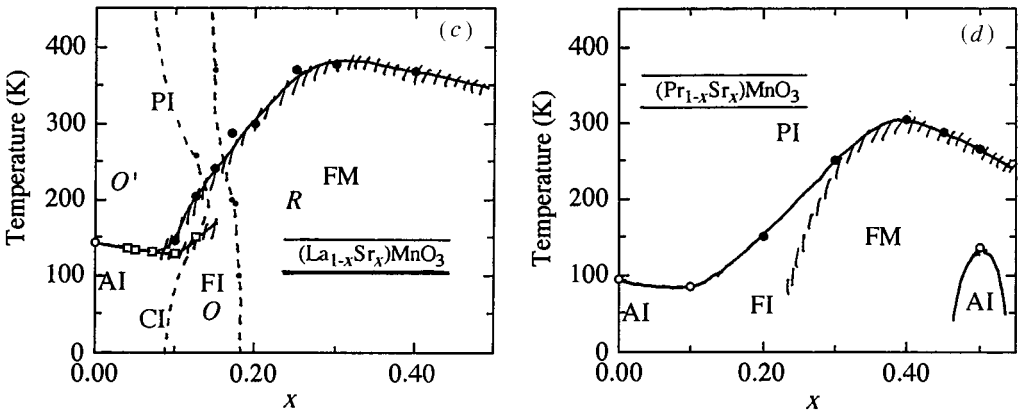

Figure 3. *Cont.* La–Sr (left) and Pr–Sr (right).

polarized 3d conduction band with two states per formula, containing one or fewer electrons. In manganites, the core is $t_{2g}^{3\uparrow}$ and the band is $e_g^{\uparrow}$; in CrO_2, the t_{2g} levels are split, the core is $t_{2g}^{\uparrow}$ and the conduction band is $t_{2g}^{\uparrow}$; in magnetite it is sufficient to consider only the octahedral B-sites; there the core is $t_{2g}^{3\uparrow}e_g^{2\uparrow}$ and the conduction band is $t_{2g}^{\downarrow}$.

Charge delocalization and ferromagnetism are closely related in these compounds, as pointed out by Zener (1951). The delocalized d electron retains its spin as it moves from core to core. As a result, the transfer integral is multiplied by a spin-dependent factor $\cos\theta_{ij}/2$ (Anderson & Hasegawa 1955), where θ_{ij} is the angle between the magnetization direction of adjacent atoms. The on-site Hund rule exchange coupling J_{H} between the core and conduction electrons is about 1 eV. Interatomic d–d correlations V are also strong, and charge-ordered states tend to form at rational fractional values of x such as 1/8, 1/2 or 3/4. The charge-ordered states are generally insulating and ferromagnetic. The ideas of orbital and charge order are illustrated schematically in figure 2. Even the ferromagnetic state is not always metallic. Because the principal energies Δ_{cf}, W, δ_{JT}, J_{H} and V are all about 1 eV, there is a variety of possible ground states. A summary of the magnitudes of the main energies involved for $LaMnO_3$ is given in table 1. U_{dd} and U_{pd} are the Mott–Hubbard and charge-transfer energies. Some typical phase diagrams are collected in figure 3, up to the limits of solid solubility. Note that there is actually no ferromagnetic metal and no metal–insulator transition in the Pr–Ca diagram, whereas it appears in all the other systems in the vicinity of $x \approx 0.3$. The differences are due in part to differences in the e_g bandwidth W, which depends sensitively on the Mn–O–Mn bond angle, which is governed in turn by cation size. Little heed has been paid to the possibility that two-phase regions separate the single-phase fields in the diagrams. Because the phases are essentially determined by the electron correlations, the likelihood is that phase segregation is on a very short lengthscale (D. Arovas & F. Guinea, unpublished work; von Molnar & Coey 1998).

Magnetic structures outside the ferromagnetic region are usually antiferromagnetic. However, a degree of random spin canting is common in the ferromagnetic phase when $x \neq 0.3$. Spin canting occurs in the A-type antiferromagnetic structure at fairly low doping levels ($x \approx 0.1$). This was predicted by de Gennes (1960) in

his seminal paper on manganites, but it is argued (Nagaev 1996) that it can be a magnetic manifestation of an electronic two-phase region.

A final point for the introduction is to emphasize the importance of disorder in the discussion of the electronic properties of manganites. The hole concentration alone does not suffice to specify the electronic properties. This point is best made by comparing non-stoichiometric magnetite (1.1) with $\delta = 0.04$, cation-doped manganite (1.2) with $x = 0.25$, and rare-earth deficient manganite

$$R_{1-z}MnO_3 \tag{1.3}$$

with $z = 0.08$. All have the same formal doping and a near-cubic crystal structure. Yet when R = La, the first is a ferromagnetic insulator, and the other two are ferromagnetic metals. The effect of potential fluctuations induced by B-site Mn vacancies on the e_g band are much more severe than those due to aliovalent substitution on the nearby A-sites, or even those due to A-site vacancies.

2. Intrinsic properties

In magnetism, it is customary to distinguish intrinsic properties, which depend only on bulk chemical composition and crystal structure, from extrinsic properties which are governed by sample size and microstructure. Hysteresis is generally an extrinsic property, spontaneous magnetization is an intrinsic one. Intrinsic properties are best measured on single crystals and epitaxial films.

(*a*) *The paramagnetic phase*

The paramagnetic insulating phase shows thermally activated conduction. The transport mechanism above T_C is still a matter of controversy as numerous groups have reported different behaviour. Data on compounds with $x \approx 0.3$ were first fitted to

$$\rho = \rho_\infty \exp(E_0/kT) \tag{2.1}$$

with an activation energy $E_0 = 0.1$–0.2 eV. Others find that Mott's variable-range hopping (VRH) expression,

$$\rho = \rho_\infty \exp((T_0/T)^\nu) \tag{2.2}$$

with $\nu = 1/4 - 1/2$ is appropriate. There is also evidence for a

$$\rho \propto T \exp(E_0/kT) \tag{2.3}$$

behaviour over an extended temperature range.

Intrinsic variations in the Coulomb potential due to the presence of A^{3+} and A^{2+} ions in the lattice, together with the presence of magnetic disorder above T_C, will lead to the formation of a *mobility edge* (Mott 1985). At high temperatures, carriers may be excited from the Fermi energy E_F to the mobility edge E_μ, giving an activated conductivity. Band transport, where E_0 is interpreted as a real gap in the density of states, is implausible, because it is difficult to justify a gap over a range of Mn^{4+} concentrations from $x = 0.2$ to 0.4 in the absence of any change in structure. But there is also a problem with interpreting E_0 as $E_\mu - E_F$. The Hall resistivity in manganites is very small and difficult to measure, but it seems that the mobility

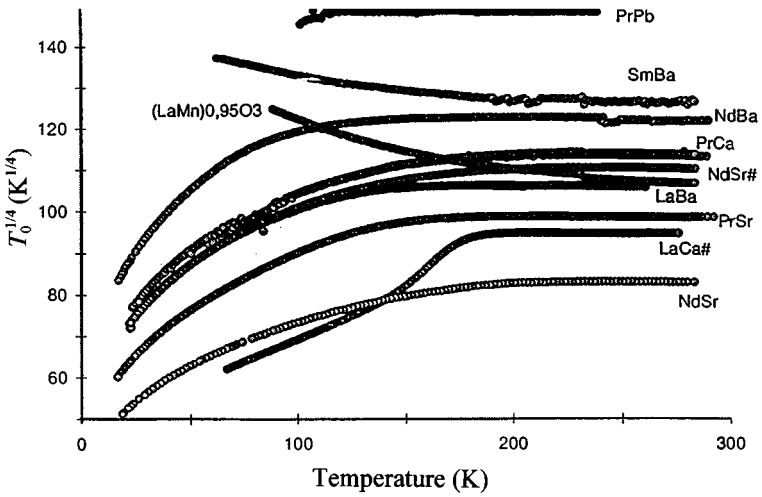

Figure 4. Plot of the parameter T_0 in the variable-range hopping model for $(R_{0.7}A_{0.3})MnO_3$ compounds with different R and A combinations.

is no more than 10^{-5} m^2 V^{-1} s^{-1}, which corresponds to a mean free path less than 0.1 nm. This is inconsistent with band transport (Hundley *et al*. 1995).

Figure 4 shows data on a series of manganites with $x = 0.3$, which have different resistivity and transition temperatures (Viret *et al*. 1997). Assuming $\nu = 1/4$ in (2.2), the VRH parameter T_0 is shown for a wide range of substituted manganites with $x \approx 0.3$. The samples were as-deposited films or bulk ceramics. With two exceptions, which were best fitted to (2.1), the curves above T_C are flat, indicating that T_0 is independent of T in that range.

Originally, the VRH theory (Mott & Davies 1971) was developed to explain electron transport in doped semiconductors, where electrons occupying hydrogenic orbitals with wavefunctions $\psi = \psi_0 \exp(-\alpha r)$ are localized by potential fluctuations associated with the dopant. Here $1/\alpha$ is the localization length. There is a competition between the potential energy difference and the distance electrons can hop. This is reflected in the expression of the hopping rate $\gamma = \gamma_0 \exp(-2\alpha R - \Delta E/kT)$ to a site at a distance R, where the energy of the carrier is ΔE higher than at the origin. Here γ_0 is a constant. Because of the exponential, the hopping rate will be dominated by the maximum value of the bracket. A sphere of radius R contains $(4/3)\pi R^3/v$ sites, where v is the lattice volume per manganese ion 5.7×10^{-29} m^3. The smallest value of ΔE is therefore $[(4/3)\pi R^3 N(E)]^{-1}$, where $N(E)$ is the density of states. Maximizing the bracket, we find $R = [(9/8)\pi a N(E) kT]^{1/4}$, hence the expression for the resistivity ($\rho \approx 1/\gamma$) is

$$\rho = \rho_\infty \exp(1.9[\alpha^3/N(E)kT]^{1/4}), \tag{2.4}$$

which is the Mott expression with

$$kT_0 = 18\alpha^3/N(E). \tag{2.5}$$

Other derivations yield different prefactors. Electron hopping is always of variable range-type at low temperature where the thermal energy is not great enough to allow electrons to hop to their nearest neighbours. In that case it is more favourable for the electrons to hop further to find a site with a smaller potential difference. At higher

temperatures, nearest-neighbour hopping ($\ln\rho \sim T^{-1}$) can contribute significantly to the transport.

To apply the model to the data in figure 4, we take the electronic density of states $N(E)$ from low-temperature heat capacity measurements (Coey *et al.* 1995) as 4×10^{28} m^{-3} eV^{-1}. Values of kT_0 (figure 2) range from 220 eV for $(La_{0.7}Sr_{0.3})MnO_3$ to 43 600 eV for $(Pr_{0.7}Pb_{0.3})MnO_3$; the corresponding localization lengths $1/\alpha$ deduced from equation (2.5) are 0.18 nm and 0.03 nm, respectively, and values of the average hopping distance at room temperature are 0.67 nm and 0.43 nm, respectively. Since the Mn–Mn distance is 0.38 nm, these numbers are incompatible with variable-range hopping associated with Anderson localization; the localization length due to random potential fluctuations must exceed the interatomic distance, and the hopping distance has to be several times greater. The discrepancy is too great to be explained by any plausible change in the density of states at T_C.

It is likely that the carriers in manganites form small dielectric polarons. There is some direct evidence of this in the distribution of Mn–O bond lengths contained in the pair distribution function of $(La_{1-x}Ca_x)MnO_3$ with $x = 0.12$ (Billinge *et al.* 1996). The hopping motion of polarons leads to a resistivity of the form of (2.3) with constant of proportionality (k/ne^2D), where n is the carrier density and D is the polaron diffusion constant. There may be contributions to the hopping energy E_0 of magnetic, elastic or Coulombic origin (Snyder *et al.* 1996*b*). Thermopower data also support polaron hopping in the paramagnetic state.

The nearest-neighbour hopping process with a high activation energy may transform into uncorrelated variable range hopping ($\ln\rho \sim T^{-1/4}$) when the available phonon energy is so small as to make the longer-range hops necessary to find a site sufficiently close in energy for hopping to occur. This is not incompatible with small dielectric polaron formation, since variable-range hopping of small polarons also leads to $\ln\rho \sim T^{-1/4}$ (Triberis & Friedman 1985). For highly correlated electron systems, a small gap appears at E_F and the hopping law is then $\ln\rho \sim T^{-1/2}$ at temperatures below the correlation gap (Efros & Shklovskii 1984).

A key question regarding the manganites concerns the relative importance of the magnetic and Coulomb random potentials in establishing the mobility edge. Manganites with $x = 0.3$ show little structural change at T_C, so that any change in band structure and density of states should be associated with the onset of ferromagnetic order. We have suggested that a random potential of mainly magnetic origin is responsible for carrier localization above T_C (Viret *et al.* 1997*a*, *b*). This potential is due to the Hund rule coupling $-J_H \boldsymbol{s}\cdot\boldsymbol{S}$ between localized Mn t_{2g} ion cores ($S = 3/2$) and the spins s of the e_g electrons in the conduction band.

We write this energy in the form $E_m = J_H(1 - \cos\theta_{ik})$, where θ_{ik} is the angle between the spins of two well-separated Mn ion cores between which the e_g electron is hopping and $2J_H$ is the splitting between spin-up and spin-down e_g bands (figure 5). Assuming the spin directions of the ion cores are uncorrelated in the paramagnetic state, the probability of finding an angle θ_{ik} between the two ion cores $P(\theta_{ik}) = \frac{1}{2}\sin\theta_{ik}$. The probability of a barrier E is therefore

$$P(E_m) = P(\theta)\frac{d\theta_{ik}}{dE_m} = \frac{1}{2U_m}. \tag{2.6}$$

Such a magnetic random potential is significant here because J_H is close to 1 eV. In estimating the density of states to include in equation (2.5), the probability of

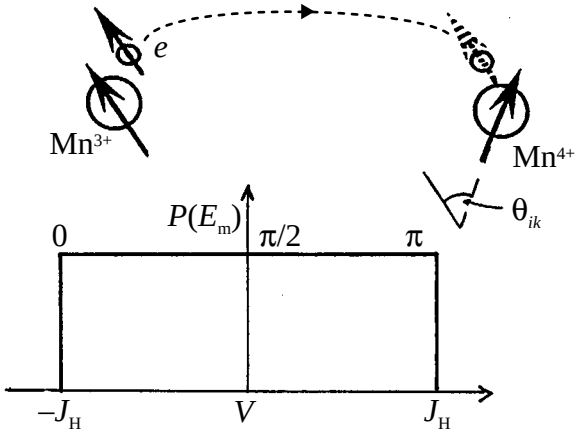

Figure 5. Variable-range electron hopping with spin memory, showing the random potential distribution of magnetic origin in the paramagnetic state. $P(E_{\mathrm{m}})$ is the probability of a hopping electron encountering an energy barrier E; J_{H} is the on-site Hund rule interaction for Mn^{3+}.

equation (2.6) must be multiplied by the number of available states per m^3. Hence,

$$N(E_{\mathrm{m}}) = P(E_{\mathrm{m}})(1-x)fg/v, \tag{2.7}$$

where $(1-x) = 0.3$ is the probability that the e_g orbital at the manganese site receiving the hopping electron is unoccupied, f is a geometric factor of order 0.5 which accounts for the fact that the hopping electron has a d_{z^2} rather than an s-state wavefunction, and g is the probability that an unoccupied manganese orbital can actually accept an electron. That $g \neq 1$ is a reflection of the dynamic Jahn–Teller effect. When ΔE is less than the Jahn–Teller stabilization energy (*ca.* 0.5 eV) associated with the tetragonal extension of the octahedron necessary to accomodate a d_{z^2} electron, a hop can only take place if the receiving site is free to distort or is already suitably distorted. Hence the value of $N(E_{\mathrm{m}})$ deduced from equations (2.6) and (2.7) is $9 \times 10^{26}\ \mathrm{m^{-3}\ eV^{-1}}$. In terms of T_0, equation (2.5) becomes $kT_0 = 342\alpha^3 J_{\mathrm{H}} v$. The corresponding localization lengths for $(La_{0.7}Sr_{0.3})MnO_3$ and $(Pr_{0.7}Pb_{0.3})MnO_3$ are 0.45 and 0.08 nm, respectively, and the average hopping ranges are 1.64 and 1.06 nm. The hopping energy $\Delta E \approx 0.1$ eV. These numbers are physically plausible since the localization length exceeds the ionic radius of Mn^{3+} and the hopping distances are 3–4 times the Mn–Mn separation.

(*b*) *The bad metal*

The ferromagnetic state in compounds with $x \approx 0.3$ is metallic in the sense that the resistivity is practically temperature-independent, with a slight positive temperature coefficient; in some cases, a slight upturn in ρ is reported below 10–20 K which can be suppressed by applied field or pressure. The conductivity is finite as $T \to 0$. But only in a few compounds such as $(La_{0.7}Sr_{0.3})MnO_3$ does the magnitude of the residual resistivity have the value expected of a metal, $\rho_0 < 1.5 \times 10^{-6}\ \Omega\,\mathrm{m}$, applying the criterion that the mean free path should exceed the interatomic spacing (Mott 1985). In other compounds, the residual resistivity can be up to ten orders of magnitude greater (Coey *et al.* 1995) making them extremely peculiar metals.

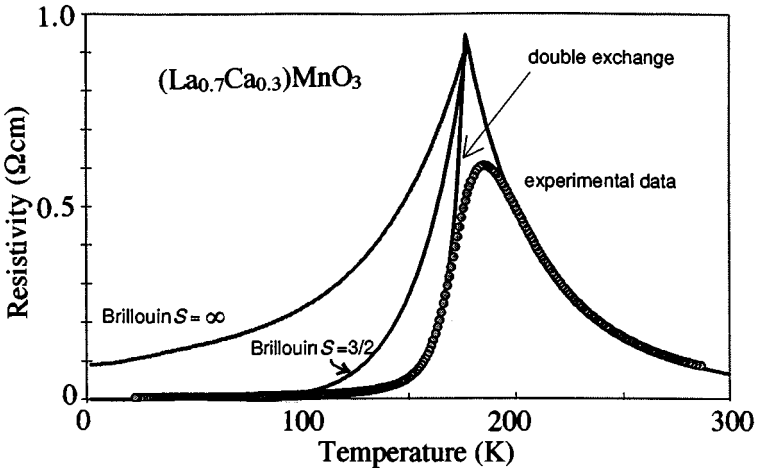

Figure 6. Comparison of the magnetic localization model with data on a $(La_{0.7}Ca_{0.3})MnO_3$ thin film. The solid curves are the resistance calculated by using the temperature dependence of the magnetization given by the Brillouin, Langevin and double-exchange models.

The resistivity in the 'bad' metallic state is unusually sensitive to pressure, with variations of ρ_0 of one order of magnitude per GPa. It is also dependent on the substrate and preparation conditions for thin films which may distort the lattice, and it depends critically on the grain size (Sánchez *et al*. 1996; Gupta *et al*. 1996) and grain-boundary angle (Kim *et al*. 1997). A variation in ρ_0 from 3×10^{-6} to $2 \times 10^{-3}\,\Omega\,\mathrm{m}$ for $(La_{0.67}Ca_{0.33})MnO_3$ has been ascribed by Gupta *et al*. (1996) to spin-dependent scattering at grain boundaries as the crystallite size decreases from bulk to 3 μm. Although grain boundaries undoubtedly play a role, the high resistivity in many of these compounds does appear to be an intrinsic property. Large reductions in ρ_0 are associated with increases in reduced magnetization (Garcia-Munoz *et al*. 1997), and it is likely that canted Mn^{4+} spins in the low temperature ferromagnetic state may account for the lack of magnetic saturation (Kaplan *et al*. 1996).

Resistivities as high as $8 \times 10^3\,\Omega\,\mathrm{m}$ are ascribed to intrinsic magnetic barriers between misaligned ferromagnetic regions which are in the nanometre size range (Coey *et al*. 1995). The electrons are delocalized in wavepackets of such small spatial extent, but must hop or tunnel from one wavepacket to the next. An inherent exponential variation in the metallic conduction with an internal parameter related to the electronic or crystal structure is needed to account for the huge variations of residual resistivity. There is an analogy with the properties of the macroscopically inhomogeneous powder compacts discussed in § 3.

(*c*) *The insulator–metal transition*

Returning to the concept of magnetic localization expressed in figure 5, the width of the band of magnetic potential fluctuations will be narrowed in an applied magnetic field, or if there is an internal molecular field, below T_C. In our view, this is the origin of the colossal magnetoresistance and the magnetically induced insulator–metal transition. The average potential is of the form:

$$\langle E_m \rangle = J_H(1 - \langle \cos\theta_{ik} \rangle). \tag{2.8}$$

If the azimuthal angle ϕ_i is randomly distributed and if θ_i are uncorrelated, then by averaging over ϕ_i it can be shown that $\langle\cos\theta_{ik}\rangle = \langle\cos\theta_i\rangle^2$, where θ_i is the angle the spins make with the applied field. The local magnetization M can also be expressed as a function of θ_i by $M = M_s\langle\cos\theta_i\rangle$, where M_s is the spontaneous magnetization. In the approximation of a square distribution of single-electron potentials with no short-range correlations, the potential width becomes $2J_H\{1-(M/M_s)^2\}$ and we obtain for T_0:

$$kT_0 = 18\alpha^3[2J_H\{1-(M/M_s)^2\}v/(1-x)fg] = 342\alpha^3 J_H\{1-(M/M_s)^2\}v. \quad (2.9)$$

Adding a residual resistivity to the resistivity given by (2.2) with $\nu = 1/4$ then gives the total temperature dependence of the resistivity, provided the temperature dependence of M_s is known. Some results of this magnetic localization model are shown in figure 6, where they are compared with data on a $(La_{0.7}Ca_{0.3})MnO_3$ thin film. The temperature dependence of M_s has be taken from classical molecular field (Langevin) theory, Brillouin theory with $S = 3/2$, or the molecular field theory of Kubo & Ohata (1972) for the double-exchange model. The only parameters involved in the fit are the Curie temperature $T_C = 200$ K and the localization length, or the product $342\alpha^3 J_H v = 4\times10^7$ K. There is excellent agreement with the Kubo–Ohata temperature dependence of magnetization, except just around T_C, where the short-range magnetic correlations have to be considered. The theory of magnetic localization outlined here could be refined by considering the magnetic correlations existing on the scale of the hopping distance (*ca.* 1 nm) rather than the averaged correlations, but the essential physics of the metal–insulator transition seems to be localization associated with magnetic disorder.

3. Micromagnetic magnetoresistance

The term 'micromagnetic magnetoresistance' is introduced to cover those low-field negative magnetoresistance effects which depend on the alignment of exchange-decoupled ferromagnetic regions in a specimen that is in some way heterogeneous.

(*a*) *Low-field magnetoresistance in manganites*

The effect in the manganites was clearly described by Huang *et al.* (1996), who compared polycrystalline $(La_{0.67}Sr_{0.33})MnO_3$ ceramics with different grain sizes with single-crystal material. Both exhibited the colossal magnetoresistance effect, but only the polycrystalline ceramics showed an additional low-field effect which becomes increasingly important at low temperatures. It was associated with spin-polarized electron tunnelling between adjacent magnetically misoriented grains. Similar effects have been observed in other polycrystalline ceramic (Gupta *et al.* 1996; Balcells *et al.* 1998; Ju & Sohn 1997) and thin-film (Snyder *et al.* 1996*a*; Shreekala *et al.* 1997; Li *et al.* 1997; Gu *et al.* 1997) manganites. The grain boundaries are about 1 nm wide. Grain boundary magnetoresistance has been isolated from colossal magnetoresistance in elegant model experiments on manganite lines deposited on a $SrTiO_3$ bicrystal substrate (Mathur *et al.* 1997; Steenbeck *et al.* 1997). Tunnel spin valves, which are sandwich structures where an insulating barrier separates two ferromagnetic layers, have a similar magnetoresistive response. A $SrTiO_3$ barrier a few nanometres thick decouples two ferromagnetic $(La_{0.7}Sr_{0.3})MnO_3$ or $(La_{0.7}Ca_{0.3})MnO_3$ layers so that

their relative magnetic orientation can be changed by a small applied field (Lu *et al*. 1996; Sun *et al*. 1996). A structure measured by Viret *et al*. (1997) shows a magnetoresistance ratio $r_{\mathrm{MR}} = \Delta R/R_0 = (R_{\max} - R_0)/R_0$ of 500% at 4 K, which is a direct indication of the high degree of spin polarization (greater than 80%) of the tunelling electrons. This is much higher than in any of the 3d metals or alloys, where the largest polarization of tunnelling electrons is 40%, for Fe (Meservey & Tedrow 1994). In both polycrystalline materials and tunnel spin valves, the resistance is maximum $R_{\max}$ at the coercive or switching field, and decreases to R_0 at saturation.

The familiar giant magnetoresistance (GMR) of metallic multilayers (Baibich *et al*. 1988) and granular metal-matrix composites (Berkowitz *et al*. 1992; Xiao *et al*. 1992) is a micromagnetic magnetoresistance effect in the sense we have defined. Resistivity is greatest at the coercive field, and decreases at technical saturation. These effects are distinct from the intrinsic magnetoresistance which depends on the bulk properties of the material. Intrinsic magnetoresistance effects include the colossal magnetoresistance discussed in § 2, anisotropic magnetoresistance (AMR) and the classical B^2 effect.

Magnetoresistance due to domain structure in the usual sense of Bloch walls in a uniform crystal is usually a very small effect, unless the walls are narrow and closely spaced (Gregg 1997). Domain wall scattering varies as δ_{w}^{-3} (G. A. Gehring & D. J. Coombes, unpublished work, 1997). Large effects only arise when there is a sharp change of magnetization direction from one ferromagnetic region or unit to the next.

(*b*) *Powder magnetoresistance*

Here we present a new approach to magnetoresistance which casts light on the physical processes involved and offers prospects of controlling the low-field, micromagnetic response. The idea is to define the ferromagnetic units and assemble them with contacts which permit spin-polarized electron transport, but not exchange coupling (other than the weak interaction mediated by the spin-polarized electron transfer). The easy way to do this is to make a powder of the ferromagnetic metallic oxide and press it into a solid pellet. We will show that remarkable magnetoresistance effects are observed in such simple 'devices'. Many developments can be envisioned such as particle surface treatment, size, shape and alignment control, incorporation of the magnetic powder into various matrices and lithographic patterning of the ferromagnetic units and their contacts. Here we focus on the simplest case of pressed powder, and illustrate the phenomenon of powder magnetoresistance (PMR) for the three oxides discussed in the introduction. In each case, powder with a certain grain size was cold-compacted in a die under a pressure of 0.3–1 GPa, and magnetization curves were measured for the fragile black pellets, together with resistivity, magnetoresistance and I–V characteristics, using a standard 4-probe DC method. The powder compacts have densities which are typically 45% of the full X-ray density.

(i) $(La_{0.67}Ca_{0.33})MnO_3$

The first example is this familiar ferromagnetic manganite. A polycrystalline ceramic was milled in a shaker mill and reduced to a particle size $d \approx 1\,\mu\mathrm{m}$. The powder was compacted under a pressure of 0.9 GPa into pellets 9 mm in diameter and less than 1 mm thick. The room-temperature resistivity of the pellet was 1.5 Ω m, which

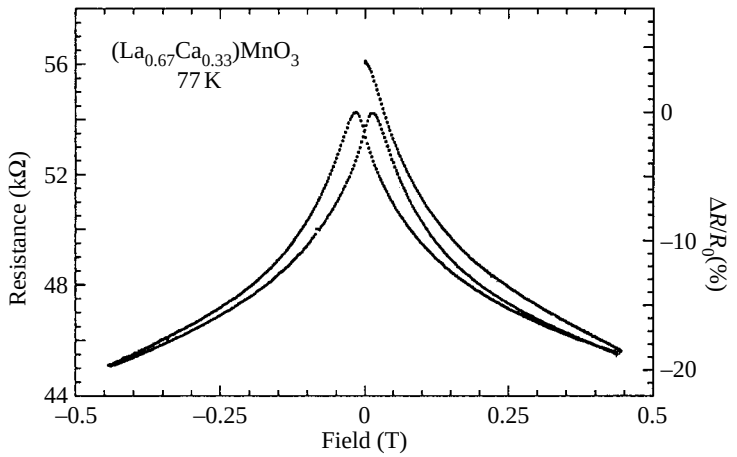

Figure 7. Magnetoresistance of a powder compact of $(La_{0.7}Ca_{0.3})MnO_3$ at 77 K, showing the virgin magnetoresistance curve.

may be compared with the intrinsic resistivity of the compound which is three orders of magnitude less, *ca.* $2 \times 10^{-3}\,\Omega\,\mathrm{m}$. The resistance is entirely due to the poor contacts between the metallic powder particles. It is possible to estimate the average resistance R_c of each contact by modelling the compact as a network of resistors in series and parallel, which gives $R_c \approx \rho/d = 1.5\,\mathrm{M}\Omega$. This crude estimate ignores the likelihood that there will actually be a very broad distribution of contact resistances, ranging from kilohms to gigohms, perhaps with a log-normal distribution. Nevertheless, it is useful to compare R_c with the quantum limit $R_q = h/2e^2 = 12.9\,\mathrm{k}\Omega$. The conductance of a metallic contact cannot be less than $1/R_q$ (Landauer 1970), so the comparison indicates whether the metallic grains are truely isolated from one another (a dielectric granular metal (Sheng 1992)) or if they are in some sort of metallic contact. In the first case, electron transport will be entirely by incoherent tunelling from grain to grain.

The low-field magnetoresistance of the manganite powder compact is shown in figure 7. The measurement at 77 K is well below the Curie point of the sample (240 K). Remarkably, there is a butterfly curve showing a magnetoresistance ratio reaching 20% in 0.5 T. The resistance is actually greatest in the virgin state, and it decreases by 20% as the field is increased to 0.5 T. Thereafter, the hysteresis loop is reversible, with the peak resistance R_{max} occurring at the coercive field. The data establish that the contact resistance is modified by the relative orientation of magnetization of contiguous particles. No clear evidence of tunnelling is observed in the I–V curves for this sample, however, because the number of particles along a conduction path between the electrodes is several thousand, and the potential drop per junction is only of order mV.

(ii) Fe_3O_4

Here we used a coarser powder, with a particle size of about 50 μm (Coey *et al.* 1998*a*). Each particle is polycrystalline and multi-domain, composed of smaller, sintered crystalline grains. For comparison, we also studied a single crystal and thin film samples which had a resistivity more than three orders of magnitude less than the

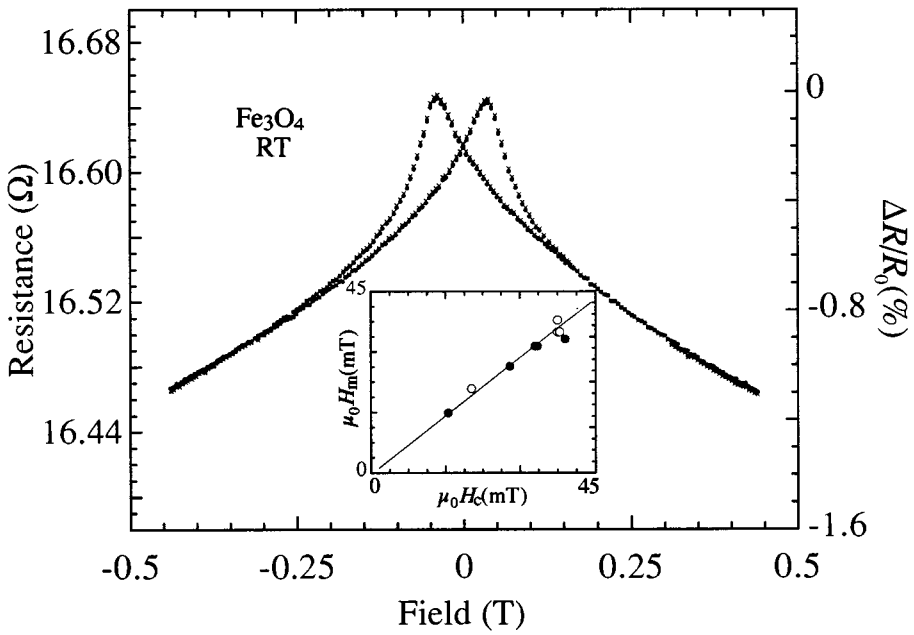

Figure 8. Room-temperature magnetoresistance of a magnetite powder compact. The insert shows how H_m, the field of maximum resistivity, corresponds to the coercivity for pressed powder (○) and polycrystalline thin films (●).

pressed powder. Magnetite has the virtue of a high Curie temperature (848 K), so that significant magnetoresistance effects (1–3%) can be observed at room temperature. Results on the pressed powder compact are shown in figure 8. The butterfly curve is again seen, with maximum resistance at the coercive field. Similar curves are found for polycrystalline films, but there is no measurable magnetoresistance on this scale in the single crystal, indicating that domain wall effects are unimportant here. R_c is estimated to be 10 kΩ at room temperature, but at lower temperatures it becomes much greater than R_q. Figure 9 shows I–V curves obtained at 130 K in fields of 2 T, where the low-field magnetoresistance is saturated, and in −15 mT where the resistivity is maximum. These have the nonlinear form expected for tunnelling through a barrier, although other intergranular transport mechanisms can also give rise to nonlinear I–V curves (Xu *et al*. 1995). An estimate of the number of junctions in a path between the voltage probes is 20, so the applied voltage per junction in figure 9 needed to increase the conductivity by a factor of 10 is approximately 300 mV. Fitting to the Simmons model for tunnelling through a square barrier (Mott & Davies 1971) gives a barrier height of 410 mV and a thickness of 2.1 nm. However, the barrier height varies inversely as the estimated number of contacts.

(iii) CrO_2

Our third example of PMR is chromium dioxide (Coey *et al*. 1998*b*). This oxide is a fairly good metal, with a residual resistivity $\rho_0 = 10^{-7}$ Ω m, and a room-temperature resistivity some 30 times greater. There is a small linear magnetoresistance, less than 1% T^{-1} around room temperature. The Curie temperature is 400 K. Single-domain

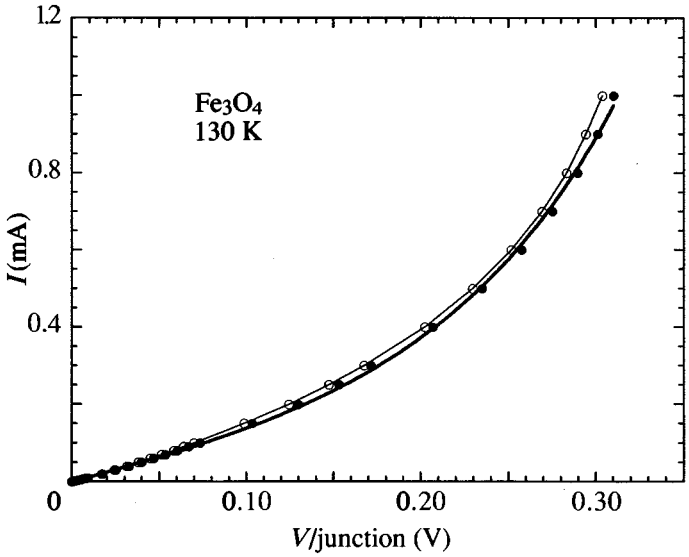

Figure 9. I–V curves for the magnetite 50 μm powder compact at 130 K. The points are taken in applied fields of 2 T (○) or −10 mT (●). The solid curve is a fit for a square tunnel barrier.

acicular particles with an aspect ratio of 10 and a length of 0.3 μm are used in magnetic recording. Cold-pressed compacts of such powder have $R_c = 30\,\mathrm{k}\Omega$. They show hysteretic magnetoresistance effects which are usually small at room temperature, but increase almost exponentially with decreasing temperature, reaching 29% at 5 K. In order to increase the sample resistance and investigate the interparticle tunnelling for powder with this very small grain size, we used the expedient of diluting the CrO_2 particles with non-ferromagnetic insulating Cr_2O_3 particles of the same size and shape, obtained by reducing the CrO_2 in vacuum. The percolation threshold for conduction in the $(CrO_2)_x(Cr_2O_3)_{1-x}$ particle mixtures is at $x = 0.23$ (by weight). We focus here on a composite with $x = 0.25$. The resistivity of the diluted compact shows the weak temperature-dependence characteristic of a granular metal in the dielectric regime (Abeles *et al*. 1975); it varies as

$$\rho = \rho_\infty \exp(\Delta/T)^{1/2}. \tag{3.1}$$

The resistivity of the diluted compact is is about $2\,\Omega\,\mathrm{m}$, three orders of magnitude more than the undiluted compact and six orders more than the intrinsic resistivity of CrO_2. Nevertheless, there is a beautiful low-field magnetoresistance effect, illustrated in figure 10, which reaches $r_{MR} = 50\%$ at 5 K and extrapolates to 56% at $T = 0$. The temperature dependence is shown in figure 11. Not only does the effect decrease with increasing temperature, it also decreases with increasing voltage applied to make the resistance measurement.

Although the number of particles in a conduction path between electrodes for this fine powder is *ca.* 10^4, a much smaller number of contacts may be expected to dominate the resistance. This is because of the broad distribution of contact resistances. Connecting all particles with $R_c < R'$ first creates small clusters with low contact resistance when R' is small. On increasing R', these clusters grow but they have to include more resistive links. Finally, at some critical value R'_{crit} the first percolation path between the electrodes appears. Further increase of R' adds

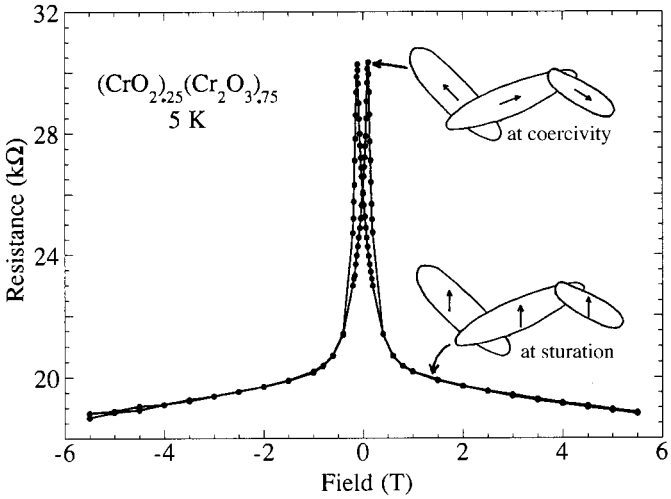

Figure 10. Magnetoresistance curve for a mixed $(CrO_2)_{0.25}(Cr_2O_3)_{0.75}$ powder compact at 5 K. The sketches show the magnetic configuration of a typical weak conduction link in a percolation path at saturation and at the coercive field.

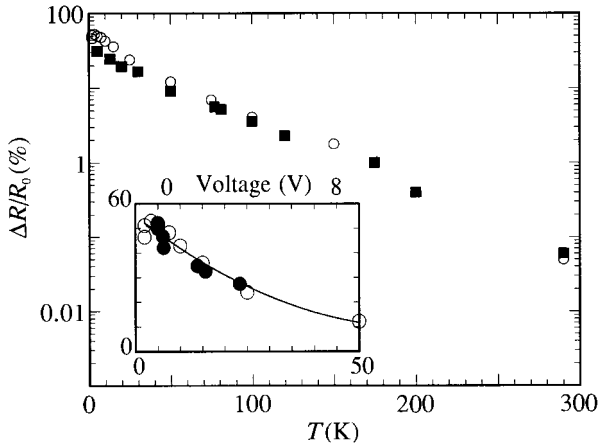

Figure 11. Temperature dependence of the magneroresistance ratio for the powder compacts CrO_2 (■) and $(CrO_2)_{0.25}(Cr_2O_3)_{0.75}$ (○). The temperature (○) and voltage (●) dependences for the same sample are compared in the inset, whence the number of weak conductance links is deduced.

extra conduction paths, but their resistance is now very high and they do little to reduce the resistivity. The resistance is therefore dominated by a fraction of weak conductance links whose resistance is *ca.* R_{crit}. An estimate of the number of particles involved is obtained by comparing the voltage and temperature dependence of the magnetoresistance ratio. Assuming the energy scales associated with temperature ($k_{\mathrm{B}}T$) and bias voltage across a single tunnel junction (eV_{b}) are equivalent, the temperature and voltage variation of $\Delta R/R_0$ in figure 11 can be reconciled by setting $4\,\mathrm{V} \equiv 25\,\mathrm{K}$, which indicates that $4e/25k_{\mathrm{B}} \approx 1900$ of these contacts are involved in the magnetotransport processes. In a another sample with a shorter distance between electrodes, this proceedure gives *ca.* 700 contacts.

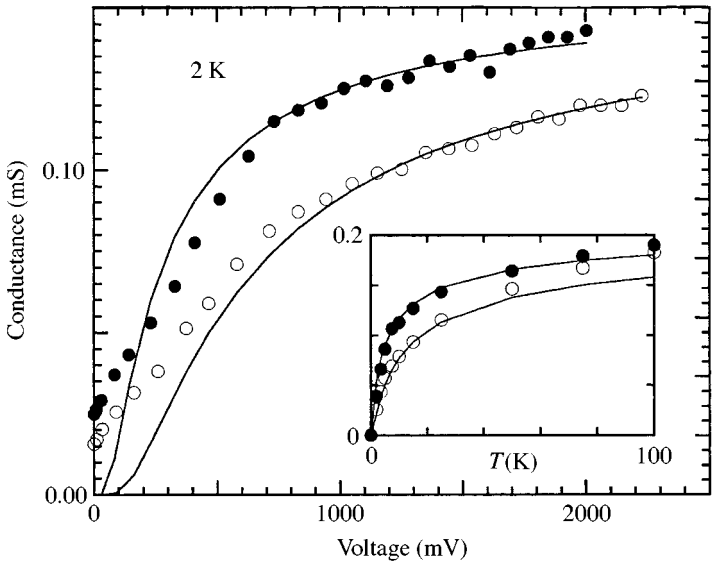

Figure 12. Conductance deduced from 2 K I–V curves of a $(CrO_2)_{0.25}(Cr_2O_3)_{0.75}$ powder compact measured in the saturated state (•) and at the coercive field (○). The solid curves are the fit to equation (3.1). The insert shows the temperature dependence of the conductance.

In order to appreciate how the high contact resistance of pressed powders can lead to high magnetoresistance, we consider a weak conductance link in the percolation path as shown in figure 10. Links in the critical path where a particle has only two neighbours and at least one relatively high-resistance contact are expected to contribute most to the measured resistivity. In fact, the resistance of the sample (6 kΩ for the $x = 0.25$ composite at room temperature) is estimated to be of similar magnitude to the resistance of the weak conductance links (Sheng 1992). The current through a weak link in a half-metallic ferromagnet is controlled by the relative orientations θ_{ij} of the magnetization of the particles. The resistance is

$$R = \frac{R_{12}}{f(\theta_{12})} + \frac{R_{23}}{f(\theta_{23})}, \tag{3.2}$$

where R_{ij} depends on the barrier height, junction area and thickness (Meservey & Tedrow 1994) and $f(\theta_{ij})$ is the relative probability of electron transfer into the adjacent particle, provided no spin depolarization occurs in the barrier, $f(0) = 1$. The general expression is (F. Guinea, unpublished work, 1998)

$$f(\theta) = \cos^2(\theta/2) + [2S/(2S+1)^2]\sin^2(\theta/2), \tag{3.3}$$

which averages to 1/2 if the orientation of the particles is random and the core spin $S \gg 1$. Hence, the resistance of the weak link varies from $2R_c$ to R_c as the magnetization of the particles is aligned and a 100% magnetoresistance ratio predicted. In CrO_2, one of the two 3d electrons is localized in a d_{xy} orbital and the other is delocalized in a half-filled conduction band (Korotin *et al.* 1998). It is therefore appropriate to take $S = 1/2$, so that $\langle f(\theta)\rangle = 5/8$ for random orientations, and the predicted magnetoresistance ratio is 60%, in good agreement with the $T = 0$ extrapolation (56%).

Another important aspect of charge transport in arrays of isolated fine particles is the Coulomb gap. The charging energy involved in transferring a single electron $E_c \approx e^2/2C$ (Abeles *et al.* 1975), where the capacitance of a particle $C = 4\pi\varepsilon_0\varepsilon r_{av}$. Taking $r_{av} = 125$ nm and an effective dielectric constant $\varepsilon = 5$, gives a charging energy of 1.2 meV (13 K). The Coulomb gap has a significant influence on the I–V curves at low temperatures. Figure 12 shows conduction derived from I–V curves measured at 2 K at the resistance peak (0.1 T) and at ferromagnetic saturation (2 T), which doubles when the voltage per contact reaches about 1 meV, and approaches a saturation value at higher voltages which is consistent with the $R(T)$ curve. The voltage-dependence of the conductance measured at 5 K and at 2 K is characteristic of a Coulomb gap, although the curves do not start at zero because the measuring temperature is comparable to the gap energy. Furthermore, the data clearly indicate a larger gap in the misaligned, coercive state than in the aligned, saturated state. Helman & Abeles (1976) first proposed an extra charging energy $E_{m'}$ of magnetic origin to explain the magnetoresistance of granular nickel. Fitting the 5 K data to their expression for fully spin-polarized electrons

$$\sigma = \sigma_0 \exp[-(E_c + E_{m'})/\mathrm{eV}], \tag{3.4}$$

where $E_{m'} = 0$ in the saturated state gives $E_c = 0.34$ mV (3.9 K), whereas in the coercive state $E_c + E_{m'} = 0.81$ mV. Hence $E_{m'} = 0.47$ mV (5.5 K). The 2 K data shown in figure 12 give $E_c = 0.29$ mV and $E_{m'} = 0.31$ mV. The magnetic energy $E_{m'}$ may be identified as the difference in exchange energy of contiguous, magnetically misaligned particles with n and n' electrons, and the same two particles with $n-1$ and $n'+1$ electrons; it is *ca.* $J/2$, where J is the interatomic exchange coupling mediated by the conduction electron. Both E_c and $E_{m'}$ are temperature dependent because tunnelling at lower temperatures is 'longer range' involving thicker (or higher) barriers but lower gaps (Helman & Abeles 1976). There is an analogy here with the variable-range hopping in doped semiconductors (Sheng 1992). PMR depends on temperature mainly because of the exchange gap. The temperature dependence of the conductivity in the disordered and saturated states is shown as an insert in figure 12, together with the curves expected from equation (3.1) setting Δ equal to the 5 K values of E_c and $(E_c + E_{m'})$. The apparent exponential variation of the magnetoresistance ratio is therefore a combination of this low-temperature behaviour together with spin flip scattering processes effective at higher temperature (F. Guinea, unpublished work, 1998). Improved magnetoresistance ratios at higher temperature can probably be be achieved by using larger particles to reduce E_c, and aligning the particles so that the magnetization of neighbours lie either parallel or antiparallel, to enhance $E_{m'}$.

The reversible, linear high-field magnetoresistance is a different physical effect, unrelated to coercivity. Its value $(1/\mu_0 R_0)(\mathrm{d}R/\mathrm{d}H) \approx 1\%/\mathrm{T}$ is also temperature and voltage dependent, but it is only half as sensitive as the magnetoresistance ratio in the CrO_2 powder compacts to changes in either temperature or voltage. It falls as $\exp(-T_{hf}/T)$ with $T_{hf} = 87$ K, whereas $\Delta R/R_0$ varies as $\exp(-T_{mr}/T)$ with $T_{mr} = 46$ K. Like the magnetoresistance, the voltage and temperature dependence can be reconciled by setting 4 V $\equiv$ 25 K in the $(CrO_2)_{0.25}(Cr_2O_3)_{0.75}$ sample, but the relevant physical processes occurring at the contacts must be different since the characteristic energy scales T_{mr} and T_{hf} differ by a factor 2. A possible explanation is that the applied field reduces the effective height or width of the tunnel barriers by modifying the width of a layer of localized charge at the surface.

4. Conclusions

We have discussed two aspects of magnetic localization in the mixed-valence manganites and related half-metallic ferromagnets. The first is an intrinsic effect associated with the fluctuating potential of magnetic origin experienced by a hopping electron in a Zener ferromagnet. The effect offers a physically plausible explanation for the metal–insulator transition and the colossal magnetoresistance. Potential fluctuations of magnetic origin lead to a temperature- and field-dependent nanometre-scale localization length.

The second effect concerns magnetic localization in small, micrometre-size ferromagnetic particles separated by tunnel barriers. The tunnelling probability is modified by a spin-dependent factor which is zero at low temperature for antiparallel magnetization alignment of contiguous particles of a half-metallic ferromagnet. The new phenomenon of powder magnetoresistance shows that large magnetoresistance ratios are associated with large contact resistances. There are good prospects for manipulating the effect by surface treatment of the powder and especially by alignment of the easy axes of the particles in a magnetic field. The coercivity of single-domain particles is quite well understood, so there are excellent prospects of achieving a desired magnetoresistance effect at room temperature by exploiting PMR.

The explanation proposed for the bad metal observed in the ferromagnetic mixed-valence manganites below T_C is analagous to that of the submicron sized granular-metal composites, but on a scale of a few nanometres. Ferromagnetic regions on this scale are separated by regions of canted spins which act as tunnel barriers.

Two aspects of the phenomena discussed here are not really understood. One is the temperature dependence of the magnetoresistance ratio, which is to some extent dependent on the magnetic gap $E_{m'}$, but is also much influenced by temperature-dependent spin-flip processes. The second is the high-field linear magnetoresistance.

The author is indebted to his collaborators at TCD, Michel Viret, Laurent Ranno and Amanda Barry, and at UCSD, Firoz Putris, Lluiz Balcells and Ami Berkowitz, without whom none of this work would have been done.

References

Abeles, B., Sheng, P., Coutts, M. D. & Arie, Y. 1975 *Adv. Phys.* **24**, 407.

Anderson, P. W. & Hasegawa, H. 1955 *Phys. Rev.* **100**, 675.

Baibich, M., Broto, J.-M., Fert, A., Dang, F. N. V., Petroff, F., Etienne, P., Creuzel, G., Friedrich, A. & Chazelas, J. 1988 *Phys. Rev. Lett.* **61**, 2472.

Berkowitz, A. E., Mitchell, J. R., Carey, M. J., Young, A. P., Zhang, S., Spada, F. E., Parker, F. T., Hutton, A. & Thomas, G. 1992 *Phys. Rev. Lett.* **68**, 3745.

Billinge, S. J. L., DiFrancesco, R. G., Kwei, G. H., Neumeier, J. J. & Thompson, J. D. 1996 *Phys. Rev. Lett.* **77**, 715.

Chahara, K., Ohno, T., Kasai, M. & Kozono, Y. 1993 *Appl. Phys. Lett.* **63**, 1990.

Coey, J. M. D., Viret, M., Ranno, L. & Ounadjela, K. 1995 *Phys. Rev. Lett.* **75**, 3910.

Coey, J. M. D., Berkowitz, A. E., Balcells, L., Putris, F. F. & Parker, F. T. 1998*a* *Appl. Phys. Lett.* **72**, 734.

Coey, J. M. D., Berkowitz, A. E., Balcells, L., Putris, F. F. & Barry, A. 1998*b* *Phys. Rev. Lett.* **80**, 3815.

Coey, J. M. D., Viret, M. & von Molnar, S. 1998*c* *Adv. Phys.* **47**. (In the press.)

de Gennes, P. G. 1960 *Phys. Rev.* **118**, 141.

Efros, B. I. & Shklovskii, A. L. 1984 *Electronic properties of doped semiconductors*. Berlin: Springer.

Fontcuberta, J., Martinez, B., Balcells, L., Obradors, X., Cohenca, C. H. & Jardin, R. F. 1998 *J. Appl. Phys.* (In the press.)

Garcia-Munoz, J. L., Fontcuberta, J., Martinez, B., Seffar, A., Pinol, S. & Obradors, X. 1997 *Phys. Rev.* B **55**, R668.

Gregg, J. F. 1997 *Phys. Rev. Lett.* **77**, 1580.

Gu, J. Y., Kwon, C., Robson, M. C., Trajanovic, Z., Ghosh, K. & Sharma, R. P. 1997 *Appl. Phys. Lett.* **70**, 1763.

Gupta, A., Gong, G. Q., Xiao, G., Duncombe, P. R., Lecoeur, P., Trouilloud, P., Wang, Y. Y., Dravid, V. P. & Sun, J. Z. 1996 *Phys. Rev.* B **54**, R15629.

Helman, J. S. & Abeles, B. 1976 *Phys. Rev. Lett.* **37**, 1429.

Hundley, M. F., Hawley, M., Heffner, R. H., Jia, Q. X., Neumeier, J. J., Tesmer, J., Thomson, J. D. & Wu, X. D. 1995 *Appl. Phys. Lett.* **67**, 860.

Hwang, H. Y., Cheong, S. W., Ong, N. P. & Batlogg, B. 1996 *Phys. Rev. Lett.* **77**, 2041.

Jonker, G. & van Santen, J. 1950 *Physica* **16**, 337.

Ju, H. L. & Sohn, H. 1997 *Solid St. Commun.* **102**, 463.

Kaplan, S. G., Quijada, M., Drew, H. D., Xiong, G. C., Ramesh, R., Kwon, C., Venkatesan, T. & Tanner, D. B. 1996 *Phys. Rev. Lett.* **77**, 2081.

Kim, K. H., Gu, J. Y., Choi, H. S., Eom, D. J., Jung, J. H. & Noh, T. W. 1997 *Phys. Rev.* B **55**, 4023.

Korotin, M. A., Anisimov, V. I., Khomskii, D. I. & Sawatzky, G. A. 1998 *Phys. Rev. Lett.* **80**, 4503.

Kubo, K. & Ohata, N. 1972 *J. Phys. Soc. Jpn* **33**, 21.

Landauer, R. 1970 *Phil. Mag.* **21**, 863.

Li, X. W., Gupta, A., Xiao, G. & Gong, G. Q. 1997 *Appl. Phys. Lett.* **71**, 1124.

Lu, Y., Li, X. W., Gong, G. Q., Xiao, G., Gupta, A., Lecoeur, P., Sun, J. Z., Wang, Y. Y. & Dravid, V. P. 1996 *Phys. Rev.* B **54**, R8357.

Mathur, N. D., Burnell, G., Isaac, S. P., Jackson, T. J., Teo, B. S., MacManus-Driscoll, J. L., Cohen, L. F., Evetts, J. E. & Blamire, M. G. 1997 *Nature* **387**, 266.

Meservey, R. & Tedrow, P. M. 1994 *Phys. Rep.* **238**, 173.

Mott, N. F. 1985 *Metal–insulator transitions*, 2nd edn. London: Taylor and Francis.

Mott, N. F. & Davies, E. 1971 *Electronic processes in noncrystalline materials*. Oxford University Press.

Nagaev, E. L. 1996 *Phys. Uspekhi* **39**, 781.

Pickett, W. E. & Singh, D. J. 1996 *Phys. Rev.* B **53**, 1146.

Ramirez, A. P. 1997 *J. Phys. Condensed Matter* **9**, 8171.

Sánchez, R. D., Rivas, J., Vasquez, C., Lopez-Quintela, A., Causa, M. T., Tovar, M. & Oseroff, S. 1996 *Appl. Phys. Lett.* **68**, 134.

Searle, C. W. & Wang, S. T. 1970 *Can. J. Phys.* **48**, 2023.

Sheng, P. 1992 *Phil. Mag.* B **65**, 357.

Shreekala, R., Rajeshwari, M., Ghosh, K., Goyal, A., Gu, J. Y., Kwon, C., Trajanovic, Z., Boettcher, T., Green, R. L., Ramesh, R. & Venkatesan, T. 1997 *Appl. Phys. Lett.* **71**, 282.

Snyder, G. J., Beasley, M. R., Geballe, T. H., Hiskes, R. & DiCarolis, S. 1996*a* *Appl. Phys. Lett.* **69**, 4254.

Snyder, G., Hiskes, R., DiCarolis, S., Beasley, M. & Geballe, T. 1996*b* *Phys. Rev.* B **53**, 14434.

Steenbeck, K., Eich, T., Kirsch, K., O'Donnell, K. & Steinbeiss, E. 1997 *Appl. Phys. Lett.* **71**, 968.

Sun, J. Z., Gallagher, W. J., Duncombe, P. R., Krusin-Elbaum, L., Altman, R. A., Gupta, A., Lu, Y., Gong, G. Q. & Xiao, G. 1996 *Appl. Phys. Lett.* **69**, 3266.

Triberis, G. P. & Friedman, L. R. 1985 *J. Phys.* C **18**, 2281.
Viret, M., Ranno, L. & Coey, J. M. D. 1997*a* *Phys. Rev.* B **55**, 8067.
Viret, M., Drouet, M., Contour, J. P., Nassar, J., Fermon, C. & Fert, A. 1997*b* *Europhys. Lett.* **39**, 545.
von Helmolt, R., Wecker, J., Holzapfel, B., Schultz, L. & Samwer, K. 1993 *Phys. Rev. Lett.* **71**, 2331.
von Molnar, S. & Coey, J. M. D. 1998 *Curr. Opinion Solid State Mater. Sci.* **3**, 171.
Xiao, J. Q., Jiang, J. S. & Chien, C. L. 1992 *Phys. Rev. Lett.* **68**, 3749.
Xu, G., Ephron, D. & Beasley, M. R. 1995 *Phys. Rev.* B **52**, 2843.
Zener, C. 1951 *Phys. Rev.* **82**, 403.

Discussion

T. Venkatesan (*University of Maryland, USA*). I have a comment relating to Professor Coey's half-metallicity arguments. We actually have experimental evidence using spin-polarized photoemission studies at Brookhaven which very clearly show that only in one spin state do you have a finite density of states at the Fermi level, literally 100% spin polarization at low temperatures in these manganites. As you go to higher temperature it drops off and approaches zero at T_C.

A. J. Millis (*The Johns Hopkins University, USA*). What does Professor Coey mean by the 'wave packet length scale' and 'localization on the wave packet length scale'?

J. M. D. Coey. By way of introduction, people have shown that as the grain size in manganites is decreased, ρ_0, the residual resistivity in Matthiessen's law, is increased. However, if you extrapolate the data beyond a grain size of perhaps 1 μm, to the resistivity for the most resistive manganites, you get an absurd value, much less than an atomic dimension. Another feature of these materials is that the ferromagnetic alignment is not perfect. So, what we suggested (Coey *et al*. 1995) is that in those very resistive ones ρ_0 can be explained in terms of some real nanoscale phase segregation. This cannot be on a very large scale because you cannot have huge fluctuations in electron density, but let's admit that the electrons are trying to segregate in little droplets. Then those regions which have more electrons in them will be ferromagnetic, and the canting is going to occur around the edges because there you have an electron deficit. Therefore, potential barriers are associated with these canted regions and you have tunnelling between the ferromagnetic wave packets. This is not like the dielectric limit of the granular metal, because we are not completely insulating; it is more like the intermediate limit of the granular metal where there is some contact at the grain boundary. The model has physical sense and it can account for the orders of magnitude. You must have something exponential controlling the metallic resistivity to explain the huge values of ρ_0.

J. R. Cooper (*University of Cambridge, UK*). Professor Coey showed a figure of $\log \Delta R/R$ versus T (figure 11) and it was nice and linear and he said it had no physical significance. But this sort of law is common in quite a lot of situations in solid state physics, like the Debye–Waller factor. Also, in charge density waves, the log of the threshold field versus temperature has the same linear behaviour.

J. M. D. Coey. I agree with the point about the Debye–Waller factor, but here we are looking at the difference between two resistances. If one or both of them were varying exponentially, that would be fine, but $\Delta R/R_0$ I think is different.

J. R. Cooper. Then this isn't any kind of magnetic decoherence equivalent to the Debye–Waller factor?

J. M. D. Coey. That may come into it, but you cannot get that linear $\log \Delta R/R$ versus T behaviour. In the model I presented, where you have the Coulomb barrier and the magnetic barrier, each ingredient contributing to the exponential variation of resistivity, they do not give an exponential temperature variation of $\Delta R/R$, it gives what I showed in figure 12, which will fit up to about 50 or 60 K, but then you have to introduce another mechanism of spin-flip scattering in order to explain why in CrO_2 you have MR effect of less than 0.1% at room temperature, yet T_C is still 400 °C.

P. C. Riedi (*University of St Andrews, UK*). With very high resistivities in these fine-grained materials, has anyone started looking at the AC resistivity? There is, for example, a huge body of data on the old sintered ferrites, where the model is essentially of capacitors weakly linked together, from which can be obtained certain characteristic properties of the system.

J. M. D. Coey. I didn't show it, but we have some beautiful Cole–Cole plots.

P. B. Littlewood (*University of Cambridge, UK*). In figure 12 showing the data on powders and fitting to a Coulomb blockade formula, I think Professor Coey was showing conductance versus bias. Whereas the theoretical model would, of course, have gone to zero conductance at zero bias, apparently the data did not.

J. M. D. Coey. The point is really that the Coulomb gap for the CrO_2 powder is only 3.9 K and the measurements were at 2 K.

D. M. Edwards (*Imperial College, London, UK*). CMR is not likely to be of practical importance because of the large fields needed to get the MR effect. What sort of field is needed to get a 5% MR effect in these powders?

J. M. D. Coey. You need more than 1 T at room temperature, much less at low temperature.

D. M. Edwards. So, once again, this is not of particularly practical importance.

J. M. D. Coey. Some would argue that you can use flux concentration to get round that, but I am unconvinced that this is practical. I think what could happen in devices is an extension of what I was discussing in terms of powder magnetoresistance. It depends on what type of devices you want to make, but you can imagine making sensors out of powder by silk-screen printing, and if you can control the powder, then you may get good properties. But if you are, say, looking for MR heads, then you must use thin films. I believe it may eventually be possible to pattern films of half-metallic ferromagnets to get large effects.

P. B. Littlewood. Is it plausible to use such high resistance devices for magnetic detection, just on the basis of the noise figures which you must have with these?

J. M. D. Coey. The resistance can be adjusted to a required value by appropriate dilution and surface treatment. I'm sure it is impractical to use the most resistive ones that we like to do the experiments on, but you can make granular films of half-metallic ferromagnets and you can imagine treating the grain boundaries to give the resistance you want.

J. Z. Sun (*IBM T. J. Watson Research Center, NY, USA*). What does Professor Coey make of the difference between the intergranular MRs in iron oxide and chromium oxide? Is it extrinsic or intrinsic, or electronic in origin? I think for Fe_3O_4 it is 0.5%, but in the chromium oxide case it is 50%. What is making the difference?

J. M. D. Coey. Let me correct Dr Sun's impression. The 50% in chromium dioxide was at 4 K. At room temperature in chromium dioxide, what I showed you was less than 0.1% and in magnetite it was less than 1.5% in the powders and in the polycrystalline films about the same. The real difference between those I think is that the Curie temperature for CrO_2 is 400 K and in magnetite it is 840 K. So if, as I suspect, the excitation of spin waves is of important to allow an electron to tunnel into a grain with the wrong magnetization, then you're better off with the highest possible Curie temperature.

J. Z. Sun. I guess Professor Coey has no data on iron oxide's low temperature magnetoresistance?

J. M. D. Coey. We do, but it doesn't become very large at low temperatures.

J. Z. Sun. My question is why?

J. M. D. Coey. I think it is most likely because of its cubic anisotropy, whereas the CrO_2 is acicular and it has uniaxial anisotropy and you have large angles between the magnetization of adjacent grains even in the powder.

J. Inoue (*Department of Applied Physics, Nagoya University, Japan*). Can the resistance of the junction be estimated in this system? Is it larger than the quantum resistance?

J. M. D. Coey. Yes, it is about four or five times larger, maybe more.

PHILOSOPHICAL TRANSACTIONS OF THE ROYAL SOCIETY A MATHEMATICAL, PHYSICAL & ENGINEERING SCIENCES

PHILOSOPHICAL TRANSACTIONS OF THE ROYAL SOCIETY A MATHEMATICAL, PHYSICAL & ENGINEERING SCIENCES